

# A Convenient and Stable Heterogeneous Nickel Catalyst for Hydrodehalogenation of Aryl Halides Using Molecular Hydrogen

David K. Leonard<sup>+</sup>,<sup>[a]</sup> Pavel Ryabchuk<sup>+</sup>,<sup>[a, b]</sup> Muhammad Anwar,<sup>[c]</sup> Sarim Dastgir,<sup>[c]</sup> Kathrin Junge,<sup>\*[a]</sup> and Matthias Beller<sup>\*[a]</sup>

Hydrodehalogenation is an effective strategy for transforming persistent and potentially toxic organohalides into their more benign congeners. Common methods utilize Pd/C or Raney-nickel as catalysts, which are either expensive or have safety concerns. In this study, a nickel-based catalyst supported on titania (Ni-phen@TiO<sub>2</sub>-800) is used as a safe alternative to pyrophoric Raney-nickel. The catalyst is prepared in a straightforward fashion by deposition of nickel(II)/1,10-phenanthroline on titania, followed by pyrolysis. The catalytic material, which was characterized by SEM, TEM, XRD, and XPS, consists of nickel

nanoparticles covered with N-doped carbon layers. By using design of experiments (DoE), this nanostructured catalyst is found to be proficient for the facile and selective hydrodehalogenation of a diverse range of substrates bearing C–I, C–Br, or C–Cl bonds (>30 examples). The practicality of this catalyst system is demonstrated by the dehalogenation of environmentally hazardous and polyhalogenated substrates atrazine, tetrabromobisphenol A, tetrachlorobenzene, and a polybrominated diphenyl ether (PBDE).

## Introduction

Halogenated organics are invaluable compounds with central importance in synthetic chemistry as solvents, carbon–carbon and carbon–nitrogen coupling reagents, and as protecting groups.<sup>[1]</sup> They offer diverse real-world applications as coolants,<sup>[2]</sup> dielectric fluids (e.g., in transformers),<sup>[3]</sup> agrochemicals,<sup>[4]</sup> and pharmaceuticals.<sup>[5]</sup> In general, the incorporation of halogen atoms into organic compounds profoundly increases both their chemical and thermal stability. This distinguishing feature has led to the widespread adoption of organohalides (particularly organobromides) in fire-retardant materials.<sup>[6]</sup>

Despite their obvious utility, organohalides can be highly damaging to animal and human health (Figure 1). This is especially well documented for halogenated dioxins – a broad class of compounds which have become infamous for their toxicity and environmental persistence. Notably, 2,3,7,8-tetrachlorodibenzo-p-dioxin (TCDD) – a byproduct from organic synthesis, and a component in Monsanto's Agent Orange herbicide used during the Vietnam War – has been linked to low sperm count in Vietnam veterans, as well as increased incidence of miscarriage in veterans' wives, and a wide variety of organ malformation in their children.<sup>[7]</sup> Moreover, dioxin-like compounds, including polychlorinated biphenyls (PCBs) and polybrominated biphenyls (PBBs) are found to be nearly impervious towards degradation, highly environmentally persistent, and have a propensity to accumulate in animal tissues. Appropriately, PCBs are now recognized as serious environmental contaminants with deleterious effects to human health,

[a] Dr. D. K. Leonard,<sup>+</sup> Dr. P. Ryabchuk,<sup>+</sup> Dr. K. Junge, Prof. Dr. M. Beller  
Leibniz-Institut für Katalyse e.V.  
Albert-Einstein-Straße 29a, 18059 Rostock (Germany)  
E-mail: kathrin.junge@catalysis.de  
matthias.beller@catalysis.de

[b] Dr. P. Ryabchuk<sup>+</sup>  
Galapagos NV  
Generaal De Wittelaan L11 A3, 2800 Mechelen (Belgium)

[c] Dr. M. Anwar, Dr. S. Dastgir  
Qatar Environment and Energy Research Institute (QEERI)  
Hamad Bin Khalifa University (HBKU)  
P.O. Box: 34110, Qatar Foundation, Education City, Doha (Qatar)

[<sup>+</sup>] These authors contributed equally to this work.

Supporting information for this article is available on the WWW under <https://doi.org/10.1002/cssc.202102315>

This publication is part of a Special Collection highlighting "The Latest Research from our Board Members". Please visit the Special Collection at [chemsuschem.org/collections](https://chemsuschem.org/collections).

© 2022 The Authors. ChemSusChem published by Wiley-VCH GmbH. This is an open access article under the terms of the Creative Commons Attribution Non-Commercial License, which permits use, distribution and reproduction in any medium, provided the original work is properly cited and is not used for commercial purposes.

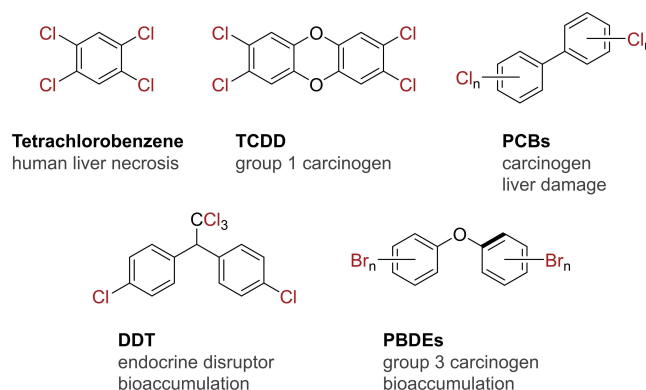


Figure 1. Examples of toxic organohalides.

especially given their extended elimination half-lives of several years within the body.<sup>[8]</sup>

Clearly, there is a real incentive to develop technologies to rid the environment of such deleterious substances. The current means for achieving this include incineration,<sup>[9]</sup> microbial degradation,<sup>[10]</sup> chemical oxidation,<sup>[11]</sup> photochemical degradation,<sup>[12]</sup> ultrasonic irradiation,<sup>[13]</sup> electrolysis,<sup>[14]</sup> and catalytic hydrodehalogenation (HDH).<sup>[15]</sup> Although incineration offers a simple solution for the treatment of chemical waste, such an approach is not appropriate in the case of (poly)halogenated organic compounds, given that their high thermal stability not only makes this highly challenging but often yields products which exhibit even greater toxicity than the initial materials.

HDH is the transformation whereby a carbon–halogen bond is formally substituted by a new carbon–hydrogen bond. For this reason, (hydro)dehalogenation has established itself as an effective strategy for detoxification and degradation of both anthropogenic and natural halide compounds.<sup>[16]</sup>

Dehalogenations of organohalides can be accomplished using (over)stoichiometric amounts of transfer hydrogenation reagents such as alcohols,<sup>[17]</sup> formic acid (or its salts),<sup>[18]</sup> metal hydride reducing agents,<sup>[19]</sup> Grignard reagents,<sup>[20]</sup> and others.<sup>[21]</sup> However, molecular hydrogen is a more attractive hydrogen donor, with wide adoption in the chemical industry, due to its considerably lower cost and higher atom efficiency than the above alternatives.

As far as transition metal-mediated HDH goes, palladium has proven to be highly effective for C–X activation and consequently this is perhaps the most common metal used for this transformation. Palladium, however, is both expensive to procure and its supply will be at risk within the next 100 years. Furthermore, Pd on charcoal requires careful treatment as it can ignite solvents and hydrogen if handled improperly. Raney-nickel (finely-ground nickel–aluminum alloy) has been demonstrated as a valued alternative.<sup>[22]</sup> Nickel has some clear benefits over palladium, including its lower cost per mole and lower potential for a supply risk in the future. On the other hand, Raney-nickel's disadvantages are its deactivation upon use and its instability. To avoid spontaneous ignition in air, it is typically stored as an aqueous slurry. It must therefore be handled with considerable care and presents a real challenge for implementation on larger scale.

In recent decades, integrating green and sustainable practices into chemical processes has become one of the central focuses in chemistry. The 12 Principles of Green Chemistry recognize the importance of catalysis for increasing efficiency, and selectivity, and realizing otherwise unfavorable reactions, whilst simultaneously reducing waste output.<sup>[23]</sup> With this in mind, coupled with our interest in sustainable redox reactions, we set out to develop a non-noble based catalyst system for HDH. Herein, we report a straightforward heterogeneous nickel nanocatalyst capable of selective dehalogenation of C–I, C–Br, and C–Cl bonds.

## Results and Discussion

### Identification of the active catalyst

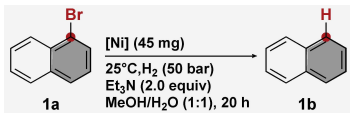
Initially a small library of 18 heterogeneous nickel-based materials was prepared in-house by using the following simple procedure: (i) heating Ni(OAc)<sub>2</sub>·4H<sub>2</sub>O and 1,10-phenanthroline monohydrate in ethanol at 60 °C to yield a nickel–phenanthroline complex; (ii) adding solid supports (SiO<sub>2</sub>, TiO<sub>2</sub>, C, SiC, CeO<sub>2</sub>, and Al<sub>2</sub>O<sub>3</sub>) to the mixture; (iii) drying the mixtures in vacuo; (iv) pyrolysis of the dried material at temperatures ranging from 600–1000 °C. Using this method of catalyst preparation, we have previously developed several iron-, cobalt- and nickel-based catalysts.<sup>[1a,24]</sup>

With the prepared materials in hand, we examined their activities for the reductive dehalogenation of 1-bromonaphthalene **1a** using molecular hydrogen and (excess) triethylamine as an HBr scavenger. After initial evaluation of all prepared catalysts under relatively mild conditions (60 °C/50 bar H<sub>2</sub>), we selected the five most active materials for assessing their performance at lower temperature (25 °C; see the Supporting Information for details). As shown in Table 1, Ni-Phen@TiO<sub>2</sub>-800 (entry 3) was the clear frontrunner, accomplishing 100% conversion of **1a** to provide a 99% yield of **1b** at ambient temperature! All the other supports (entries 1, 2, 4 & 5) led to both lower yields and selectivities, with tetralin as a side-product. Notably, the effectiveness of pyrolyzing at 700–800 °C is consistent with several of our previously described heterogeneous catalysts.<sup>[1a,24b–f]</sup>

### Experimental design

Having identified a suitable catalyst, we set about optimizing the reaction conditions to minimize reagent and catalyst use whilst maintaining high reactivity under mild conditions. Since there are several variables which could influence the product yields of our catalytic system, we opted to utilize design of experiments (DoE) for a robust and expedient multivariate analysis of the reaction parameters. In contrast to univariate (i.e., one-factor-at-a-time) analyses, DoE can encompass a large volume of chemical space and reveal which factors – and

**Table 1.** Investigation for catalytically active materials<sup>[a]</sup>

			
Entry	Ni-Phen@support-pyrolysis T	Conversion <sup>[b]</sup> [%]	Yield <sup>[b]</sup> [%]
1	Ni-Phen@C-800	31	26
2	Ni-Phen@TiO <sub>2</sub> -600	39	22
3	Ni-Phen@TiO <sub>2</sub> -800	100	99
4	Ni-Phen@TiO <sub>2</sub> -1000	44	32
5	Ni-Phen@Al <sub>2</sub> O <sub>3</sub> -1000	32	26

[a] Reaction conditions: 0.5 mmol **1a**, 45 mg of catalyst, Et<sub>3</sub>N (2.0 equiv), 50 bar H<sub>2</sub>, 25 °C, 2 mL MeOH/H<sub>2</sub>O (1:1), 20 h. [b] Conversion and yield determined by GC-FID using *n*-hexadecane as an internal standard.

interactions between factors – have the largest influence on the reaction outcome (e.g., yield, selectivity). We selected four different reaction parameters ( $T$ ,  $p$ , catalyst loading, and base loading) to examine for the reductive dehalogenation of **1a**.

A two-level full-fractional investigation ( $2^4$  design) of temperature, pressure, catalyst loading, and amount of base entailed a total of 20 reaction runs, including the runs performed in the center of the design space (performed in quadruplicate). Using an analysis of variance (ANOVA), we were able to identify the reaction parameters which were statistically significant (i.e., those which had  $p$ -values below the 0.05 threshold) within the investigation range (Table S7). Accordingly, the statistically significant parameters we observed are: (i) amount of base, (ii) catalyst loading, and (iii) temperature. Significant interactions were also detected between (iv) catalyst loading and temperature, as well as (v) catalyst loading and amount of base. Contour plots (Figure 2 and the Supporting Information) reveal the interactions between factors and highlight the most favorable areas of chemical space. In this fashion, we were able to achieve full conversion of **1a** and 92% yield of **1b** after 18 h at 45 °C, using just 20 bar  $H_2$  and a slight excess of triethylamine (1.25 equiv).

The important role of the base is not surprising in this reaction for two reasons: firstly, as the reaction progresses, a bromine atom is displaced from the substrate to form acidic HBr, and secondly, we have previously observed that  $NEt_3$  can assist with the heterolytic cleavage of molecular hydrogen.<sup>[24e]</sup>

### Reaction scope and limitations

To examine the scope of the HDH reaction, we subjected more than 30 aryl bromides and aryl chlorides to our optimized catalyst system (Scheme 1). In general, we observed that the electron-rich and weakly electron-deficient substrates **1a**–**6a** are favoured in this reaction and dehalogenation was possible under mild conditions (20 bar  $H_2$ , 45–60 °C) with good to excellent yields (80 to >99%). In contrast, harsher reaction conditions were necessary for amine **7a** and electron-deficient aryl bromides **8a**–**16a**, as well as for all aryl chlorides. Notably, by moderating the reaction temperature, we were able to promote chemoselective dehalogenation of anisoles **2a** and **5a**,

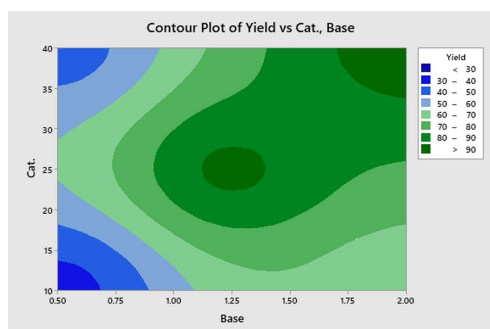
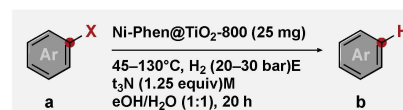
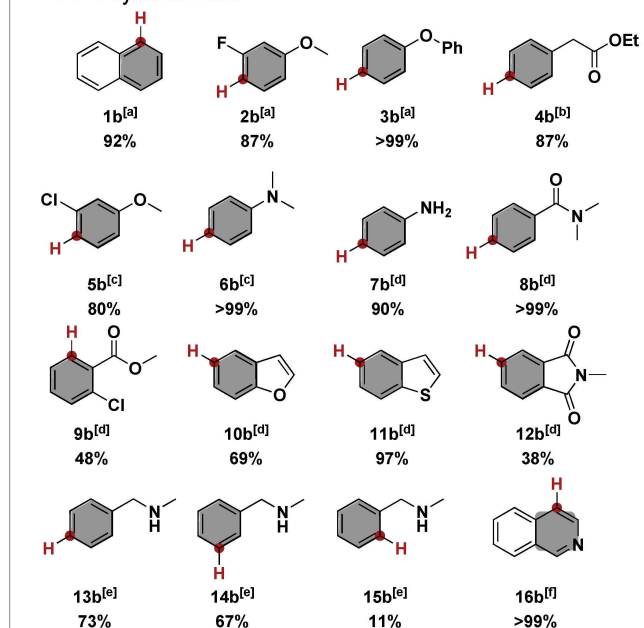


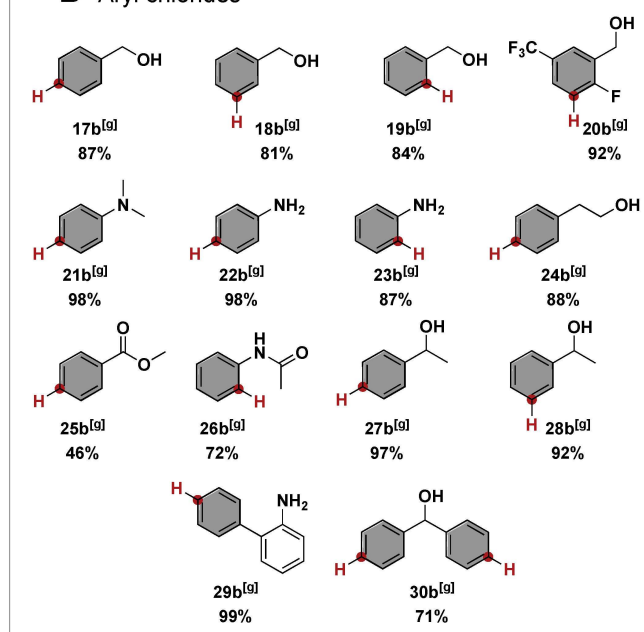
**Figure 2.** Contour plot from the DoE showing interaction between catalyst loading and base.



### A Aryl bromides



### B Aryl chlorides



**Scheme 1.** HDH of aryl halides: [a] Reaction conditions: 0.5 mmol **a**, 25 mg of Ni-Phen@TiO<sub>2</sub>-800 (ca. 3 mol % Ni), Et<sub>3</sub>N (1.25 equiv), 20 bar  $H_2$ , 45 °C, 2 mL MeOH/ $H_2$ O (1:1), 20 h, full conversion of **a** and yields determined by GC-FID using *n*-hexadecane as an internal standard; [b] 50 °C, 2 mL EtOH: $H_2$ O (1:1); [c] 60 °C; [d] 80 °C; [e] 90 °C, 30 bar  $H_2$ , full conversion of **13a** was achieved; [f] 120 °C, 30 bar  $H_2$ ; [g] 130 °C, 30 bar  $H_2$ .

which bear more than one halide atom. At 90 °C and 30 bar  $H_2$  pressure, a decrease in HDH yield of 6% and 65% was observed for phenylmethanamines **13a**–**15a** upon moving the bromine

atom from *para*- to *meta*-, and *meta*- to *ortho*-positions, respectively. This is likely caused by the decreased proximity between the inductively withdrawing methylmethanimine and the bromine atom, or due to increased steric bulk at the reaction center.

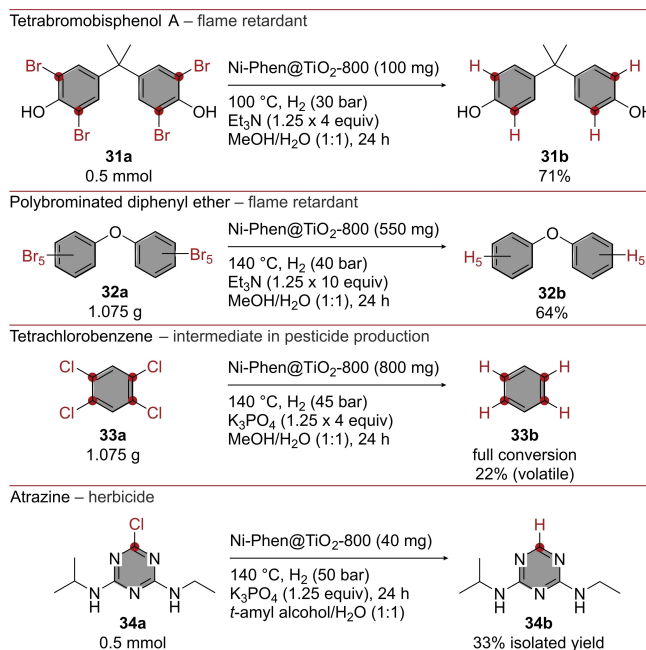
HDH of heterocyclic compounds is pertinent in the degradation of pharmaceutical and agrochemical ingredients. With this in mind, representative heterocycles 4-bromo-1-benzofuran **10a** and 4-bromobenzo-1-furanthiophene **11a** were hydrodehalogenated to the corresponding congeners in 69% and 97% yield, respectively, at 80 °C and 20 bar H<sub>2</sub> pressure. In contrast, isoindoline **12a** proved to be more challenging under these conditions, with only a modest 38% yield of the expected product. Similarly, 4-bromoisquinoline **16a** was found to be a particularly challenging substrate, however, an increased temperature of 120 °C furnished the product with quantitative yield.

Ethyl ester **4a** was incompatible with our solvent system of methanol and water (1:1) (which had previously shown compatibility with catalysts of this type)<sup>[24a]</sup> due to transesterification to yield the corresponding methyl ester. However, upon switching to aqueous ethanol (40%), this issue was easily resolved leading to an 87% yield of **4b**. We also found that this reaction occurs smoothly in a variety of alcoholic beverages with similar alcohol content (Table S8). Besides obtaining a low dehalogenation yield for substrate **25a** (46%), which contains an electron-withdrawing methyl ester substituent, all aryl chlorides tested were transformed in good to excellent yields (71–99%) at 130 °C under 30 bar H<sub>2</sub>.

## Applications

To demonstrate the efficacy of our reaction for degradation of thermally inert substances, we subjected tetrabromobisphenol A **31a** – a widely applied fire retardant and a precursor for fire-resistant polymers – to our Ni-Phen@TiO<sub>2</sub>-800 catalyst. At 100 °C full dehalogenation of all four bromine atoms was achieved giving 71% yield of the expected product **31b**. This transformation attests to the nickel catalyst's ability to take highly stable compounds, which are resistant to degradation, and transform them into substances more readily treated and disposed of. Furthermore, the upscaling of the catalytic protocol was successfully demonstrated in 5 mmol-scale reactions of the two industrially relevant compounds **32a** and **33a** (Scheme 2). Substrate **32a** represents the class of polybrominated diphenyl ethers (PBDEs) which are recognized as persistent organic pollutants that bioaccumulate in different organisms due to their low degradation. 1,2,4,5-Tetrachlorobenzene **33a** is a widely used precursor in the production of herbicides and the HDH demonstrates the catalyst's capability of activating multiple C–Cl bonds in a clean and efficient manner.

Syngenta's atrazine **34a** is a pre-emergent herbicide that is widely applied in the United States and Australia for broad spectrum weed control. Despite its continued operation today, it has been banned in the European Union since 2004 due to its concentrations in groundwater which exceeded regulatory limits. Moreover, this chlorinated triazole remains persistent in



**Scheme 2.** HDH of tetrabromobisphenol A **31a**, PBDE **32a**, 1,2,4,5-tetrachlorobenzene, and atrazine.

both groundwater and in soil for up to four years.<sup>[25]</sup> Here, HDH of the C–Cl bond in **34a** was achieved using catalytic amounts of Ni-Phen@TiO<sub>2</sub>-800 to yield the corresponding product **34b** isolated in 33% yield.

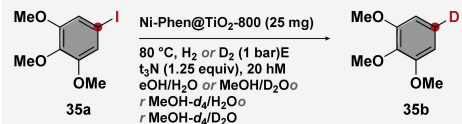
Raney-nickel is well known for its ability to dehalogenate organohalides. We became interested in studying the reductive dehalogenation of **1a** and comparing our best results using Ni-Phen@TiO<sub>2</sub>-800 with Raney-nickel slurry. Using 10 mg of Raney-nickel slurry proved effective for this transformation and led to an 84% yield of **1b**, with no detectable side products. But increasing amounts of Raney-nickel led to a reduction in yield and drop in selectivity as hydrogenation of one aromatic ring yielded tetralin as a co-product (Section S12). Preferential selectivity for tetralin was observed, when the slurry was added in larger amounts (100–250 mg) with no detection of **1b**. Notably, even high loading (100 mg) of our Ni-Phen@TiO<sub>2</sub>-800 catalyst completely prevented any tetralin formation.

Apart from catalytic HDH reactions, such a catalytic system can be considered for similar deuterodehalogenation (DDH) transformations. Indeed, there is an ongoing high interest in developing new deuteration methods, as isotope labelling plays an essential role for drug development. In detail, deuteration of active drugs can benefit their properties by significantly reducing rates of metabolism, leading to less frequent dosing to achieve the same therapeutic effects.<sup>[26]</sup>

Accordingly, we explored DDH for achieving deuterium incorporation. Using 5-iodo-1,2,3-trimethoxybenzene **35a**, which undergoes full dehalogenation with Ni-Phen@TiO<sub>2</sub>-800 using just 1 bar H<sub>2</sub> at 80 °C, we tested various deuterium sources for selective D-labeling at the 5-position on the benzene ring (Table 2). We observed low to modest D



Table 2. Deuteration of 5-iodo-1,2,3-trimethoxybenzene.<sup>[a]</sup>

				
Entry	Solvent A	Solvent B	Reductant (1 bar)	D incorp. [%]
1 <sup>[b]</sup>	D <sub>2</sub> O	MeOH	H <sub>2</sub>	49
2 <sup>[b]</sup>	H <sub>2</sub> O	MeOH- <i>d</i> <sub>4</sub>	H <sub>2</sub>	9
03 <sup>[b]</sup>	D <sub>2</sub> O	MeOH- <i>d</i> <sub>4</sub>	H <sub>2</sub>	86
4	H <sub>2</sub> O	MeOH	D <sub>2</sub>	no reactivity
5	D <sub>2</sub> O	MeOH	D <sub>2</sub>	no reactivity
6	H <sub>2</sub> O	MeOH- <i>d</i> <sub>4</sub>	D <sub>2</sub>	no reactivity
7	D <sub>2</sub> O	MeOH- <i>d</i> <sub>4</sub>	D <sub>2</sub>	no reactivity
8 <sup>[c]</sup>	D <sub>2</sub> O	MeOH- <i>d</i> <sub>4</sub>	D <sub>2</sub>	no reactivity
9 <sup>[d]</sup>	D <sub>2</sub> O	MeOH- <i>d</i> <sub>4</sub>	–	no reactivity

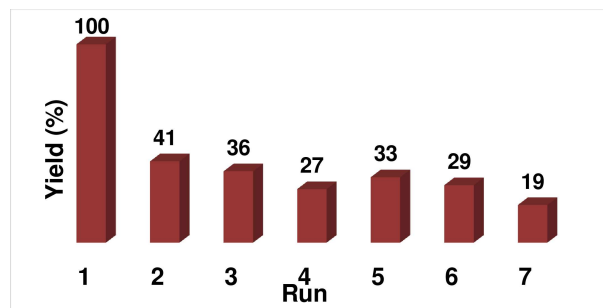
[a] Reaction conditions: 0.5 mmol **35a**, 25 mg of Ni-Phen@TiO<sub>2</sub>-800 (ca. 3 mol % Ni), Et<sub>3</sub>N (1.25 equiv), 1 bar H<sub>2</sub> or D<sub>2</sub>, 80 °C, 2 mL solvent mixture (1:1), 20 h. [b] Full conversion of **35a** was reached. [c] 10 bar D<sub>2</sub> was used. [d] The reaction autoclave was purged and backfilled with Ar, instead of H<sub>2</sub> or D<sub>2</sub>.

incorporation using MeOH-*d*<sub>4</sub> and D<sub>2</sub>O, respectively, under an atmosphere of hydrogen. Nevertheless, we found that very high D incorporation (86%) could be realized when both MeOH-*d*<sub>4</sub> and D<sub>2</sub>O were used simultaneously. To our surprise, switching from hydrogen to deuterium gas led to no improvement in deuteration; in fact, no reactivity was observed at all and only starting material could be recovered from the reaction vessel. This observation can be explained by the increased bond strength of D–D compared to H–H, resulting in impeded bond cleavage. From these data, we infer that the D<sub>2</sub>O is the most effective deuterium source for deuteration of **35a**. From a practical point of view, it is important to note that D<sub>2</sub>O is relatively inexpensive (as D-sources go) and it is the parent compound of other D-sources, including D<sub>2</sub>.

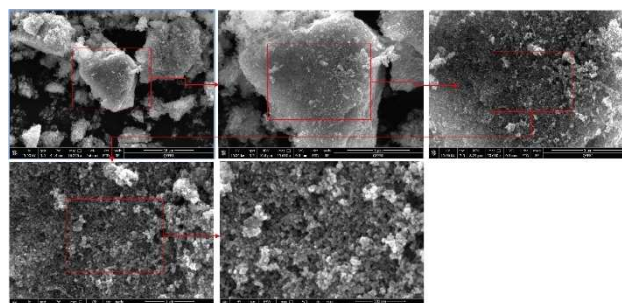
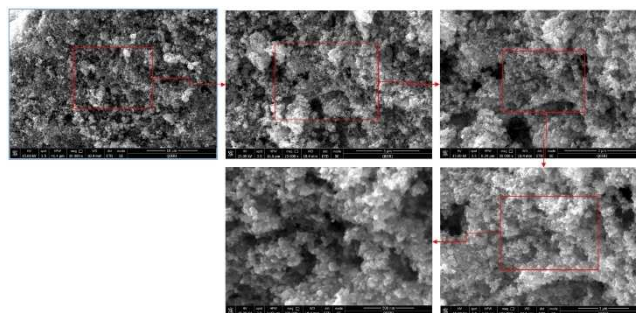
## Recyclability

Catalyst stability and recyclability is undoubtedly an important consideration for heterogeneous catalysts. Accordingly, the activity of the Ni-Phen@TiO<sub>2</sub>-800 catalyst was monitored over seven consecutive dehalogenations of **1a** using our optimized reaction conditions. From Figure 3, we see that, whereas a quantitative yield of **1b** was achieved on the first run, subsequent reuse during the second run provided a significantly lower yield of 41%. Thereafter, the activity was maintained, and more consistent yields were then obtained during consecutive runs, and 19% yield of **1b** was still obtained after the seventh run.

Due to the observed decrease in the catalyst's activity, we initially hypothesized that nickel may be leaching into the reaction solution. Thus, each reaction solution was analyzed by inductively coupled plasma mass spectrometry (ICP-MS) to look for the presence of any nickel. To our surprise, and despite the very low detection limit of the instrumentation, no nickel was detected. The change in reactivity therefore suggested that

Figure 3. Recycling Ni-Phen@TiO<sub>2</sub>-800 for HDH of **1a**.

there were structural changes in the catalyst, most noticeably, after the first run. Thus, scanning electron microscopy (SEM) analyses for Ni-Phen@TiO<sub>2</sub>-800 were conducted for both fresh (Figure 4) and spent catalyst samples (Figure 5). The SEM analyses showed three-dimensional nanoparticle agglomerations for the fresh catalyst. These nanoparticles have an average size in the range of 9.82–50.3 nm. The main discernible difference from the high-resolution SEM images for the fresh and spent catalyst is the randomly oriented nature of these particles with variable length thickness of the nanoparticles. Compositional analysis by energy dispersive X-ray spectroscopy (EDX)-elemental mapping reveals a widespread distribution of nickel and carbon throughout the titania matrix. It is understood that the structural changes in the catalyst are responsible for the drop in reactivity upon its reuse.

Figure 4. SEM images of the fresh Ni-phen@TiO<sub>2</sub>-800 catalyst.Figure 5. SEM images of the spent Ni-phen@TiO<sub>2</sub>-800 catalyst.

### Characterization of the active catalyst

The Ni doped titania catalyst was characterized by means of X-ray powder diffraction (XRPD) to probe the crystallite structure of the material. Figure S2 shows the presence of a mixture of rutile and anatase  $\text{TiO}_2$  phases, with anatase as the dominate phase. The reflections at  $2\theta$  values of 25.31, 37.84, 48.06, 53.98, 55.12, 62.72, 68.14, 70.26, 75.14, and 82.76 are characteristic for the anatase phase, matching with the standard pattern JCPDS 21-1272.<sup>[27]</sup> Whereas, the peaks at  $2\theta$  values 27.44, 36.06, 41.14, and 56.56 were unambiguously assigned to the rutile phase matching with JCPDS 21-1276.<sup>[27b,28]</sup> The rutile titania phase has been reported to be predominant at a higher processing temperature and is usually obtained through high temperature calcination of anatase-phase  $\text{TiO}_2$ .<sup>[29]</sup> The reflections at  $2\theta$  values of 44.50 and 51.84 correspond to the FCC-phase of Ni.<sup>[30]</sup> The crystallite size was calculated by using the Scherrer equation  $D = k\lambda/\beta\cos\theta$ , where  $D$ =average crystallite size,  $K$ =Scherrer coefficient,  $\lambda$ =wavelength of X-ray radiation,  $\theta$ =diffraction angle, and  $\beta$ =FWHM of diffraction peak, which is reflected in the observed broad reflections in the XRD spectrum of the catalyst sample shown in Figure S2.

For further characterization, the catalyst was analyzed using X-ray photoelectron spectroscopy (XPS), scanning electron microscopy (SEM), and transmission electron microscopy (TEM). Near-surface elemental compositions and the oxidation states of the metal in fresh and spent catalysts were analyzed using XPS in the binding energy region 0–1400 eV. The survey spectrum for fresh catalyst shown in Figure 6a reveals the presence of Ni, O, Ti, N, and C in the Ni-Phen@ $\text{TiO}_2$ -800 matrix. The binding energy was corrected by setting the C 1s peak from adventitious hydrocarbon at 284.8 eV. The Ni 2p spectrum (Figure 6b) shows the peaks at binding energy of 855.59 eV and

873.80 eV which are characteristic peaks assigned to  $\text{Ni}2p_{3/2}$  and  $\text{Ni}2p_{1/2}$ , respectively. Both peaks accompanied by their satellite peaks at binding energies of 860.66 and 879.02 eV, respectively. The deconvoluted Ni  $2p_{3/2}$  peak at 855.59 eV corresponds to NiO, and the 857.53 eV peak corresponds to  $\text{Ni}(\text{OH})_2$ .<sup>[31]</sup> The peak located at 853.02 eV is attributed to  $\text{Ni}^0$  which indicates the presence of metallic nickel on the catalyst surface.<sup>[32]</sup> The atomic distribution of 1.25:1.0 for  $\text{Ni}^{2+}$ :  $\text{Ni}^0$  was quantified using the spectral intensity of  $\text{Ni}2p_{3/2}$  and  $\text{Ni}^0$  peaks of the XPS spectrum. The deconvolution of the C 1s spectrum (Figure 6c) shows relevant fitting peaks with the binding energies at 284.77 eV for  $\text{C}(\text{sp}^3)\text{--C}(\text{sp}^3)$ , 286.10 eV for  $\text{C}(\text{sp}^3)\text{--O}$ , and 287.97 eV for  $\text{C=O}$ .

The first peak at 284.77 eV was attributed to the adventitious elemental carbon on the surface, whereas the other two peaks are from C–O (C–O–C) and C=O are assigned to oxidized carbon species.<sup>[33]</sup> Moreover, the absence of a peak around 282.0 eV reveals that the substitution of oxygen in the lattice of  $\text{TiO}_2$  as Ti–C is not formed.<sup>[33c,d]</sup> In the O 1s spectrum (Figure 6d), the large peak at 530.40 eV is assigned to a metal–O bond and the peak at 531.90 eV was assigned to C–O.<sup>[34]</sup> This indicates different chemical states of oxygen on the surface of catalyst.

In the N 1s XPS spectrum (Figure 6e), the deconvolution of the N 1s region revealed the presence of peaks at 399.20 eV and 401.30 eV attributed to pyridinic-N and graphitic-N respectively.<sup>[35]</sup> The Ti 2p spectrum indicates two photoelectron signals  $\text{Ti}2p_{3/2}$  and  $\text{Ti}2p_{1/2}$  with binding energies at 458.98 and 464.80 eV, respectively, and an associated satellite peak at 472.51 eV.<sup>[33d,36]</sup>

Scanning electron microscopy (SEM) images reveal the surface morphology of the catalyst before the reaction. These images show the presence of small spherical particles which are agglomerated together, whereas widely dispersed spherical

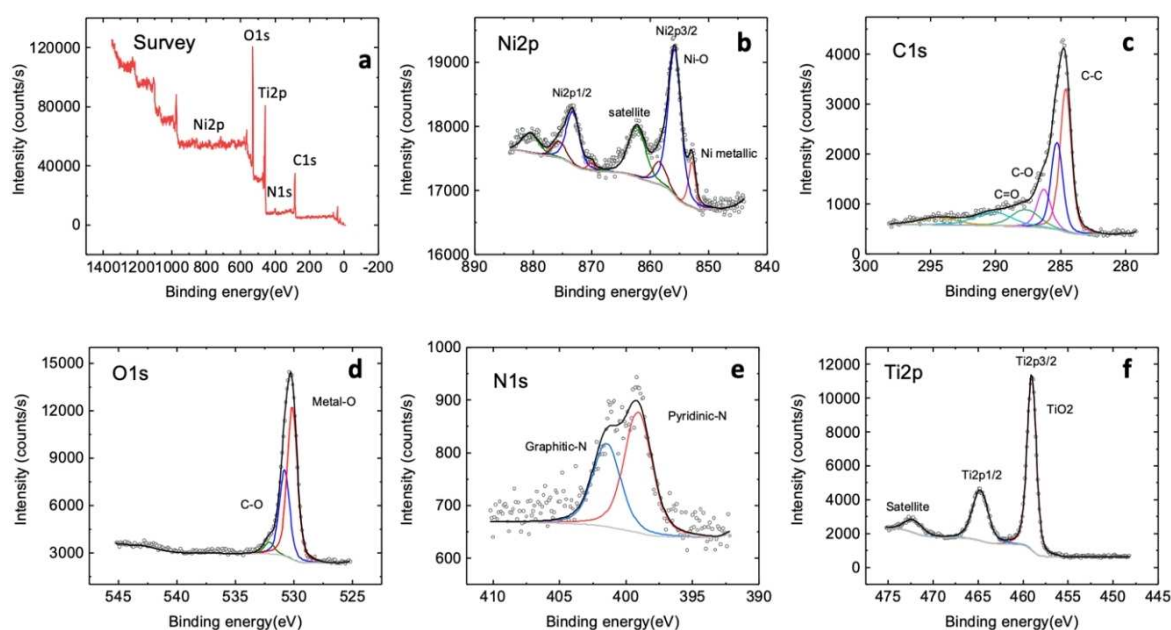


**Figure 6.** XPS survey spectrum of Ni-Phen@ $\text{TiO}_2$ -800 catalyst (a) and high-resolution deconvoluted XPS spectra for Ni 2p (b), C 1s (c), O 1s (d), N 1s (e) and Ti 2p (f).

particles are predominantly observed for the spent catalyst samples (Figures 4 and 5). The EDS spectra for the catalyst before and after the reaction are shown in Figure S11.

## Conclusion

We have developed safe and inexpensive Ni-Phen@TiO<sub>2</sub>-800 as a catalyst for the dehalogenation of aryl iodides, bromides, and chlorides. This catalytic system allows for HDH of various substrates incorporating electron-rich and electron-poor groups, sensitive functional groups, and heterocycles. The utility of this heterogeneous nickel catalyst was demonstrated on gram-scale HDH of more challenging and industrially relevant substrates, such as environmentally persistent fire retardants, toxic polybrominated diphenyl ethers (PBDEs), and 1,2,4,5-tetrachlorobenzene. Furthermore, we have showcased that this catalyst system could be used for selective incorporation of deuterium labels by using D<sub>2</sub>O/methanol-*d*<sub>4</sub> as a deuterium source. Compared to commercial Raney-nickel, our easy-to-handle nickel catalyst provides higher HDH yields under the same conditions without byproduct formation.

## Experimental Section

### Synthesis of the Ni-Phen@TiO<sub>2</sub>-800 catalyst

A 250 mL oven-dried single-necked round-bottomed flask equipped with a reflux condenser and a Teflon-coated, egg-shaped magnetic stir bar (40×18 mm) was charged with Ni(OAc)<sub>2</sub>·4H<sub>2</sub>O (373.3 mg, 1.5 mmol, 1.0 equiv), 1,10-phenanthroline monohydrate (594 mg, 3.0 mmol, 2.0 equiv) and dissolved in ethanol (60 mL). After stirring for 5 min at 25 °C, the flask was immersed in an oil bath and heated at 60 °C for 2 h. To the reaction mixture 2.10 g of TiO<sub>2</sub> was added via a glass funnel and the resulting heterogeneous mixture was stirred at 750 rpm for 2 h at 60 °C. The flask was taken out from the bath and cooled to ambient temperature. The solvent was removed slowly in vacuo (180 mbar, bath temperature 40 °C, 200 rpm), then dried in vacuo (ca. 1.0 mmHg, 23 °C) for 14 h to give a light blue-green solid. Using a mortar and pestle, the sample was ground to a fine powder which was then transferred to a ceramic crucible (height=20 mm, top Ø=40 mm) and placed in an oven. The latter was evacuated to ca. 5 mbar and then flushed with argon three times. The furnace was heated to 800 °C at a rate of 25 °C per min and held at 800 °C for 2 h under an atmosphere of argon. After the heating was switched off, the oven was allowed to reach room temperature, giving the Ni-phen@TiO<sub>2</sub>-800 catalyst as a dark blue-black powder (Note: during the whole process argon was constantly passed through the oven). Elemental analysis: 3.23 % N 1.56 % N 12.70 % C.

### General procedure for HDH of aryl halides

An 8 mL glass vial (Ø=14 mm, height 50 mm) equipped with a Teflon-coated oval magnetic stirring bar (8×5 mm) was charged with Ni-phen@TiO<sub>2</sub>-800 (25 mg) before the vessel was sealed with a plastic screw cap bearing a silicone septum. The silicone septum was then punctured with a 26-gauge syringe needle (0.45×12 mm). Aryl halide (0.5 mmol) and triethylamine (88 µL, 0.625 mmol, 1.25 equiv) were then added via a 100 µL microsyringe. Deionized water (1 mL) and methanol (1 mL) were then added before the vial

was placed into a small aluminum plate which was then transferred into a 300 mL steel autoclave (Parr Instrument Company). Once sealed, the autoclave was placed into a large aluminum heating block and purged 3 times with hydrogen (at 5–10 bar). Next the autoclave was pressurized with hydrogen (20–30 bar) and heated (45–130 °C) with thorough stirring (700 rpm). After 20 h, the autoclave was removed from the large aluminum block and cooled to room temperature in a water bath. The remaining hydrogen was discharged and the vials containing reaction products were removed from the autoclave. Ethyl acetate (6 mL) was added to the reaction vial and the resulting mixture was stirred intensively for 30 s. The solid catalyst was then separated by centrifugation and the liquid phase was analyzed by GC-FID to quantify the yield of the dehalogenated product, using *n*-hexadecane as an internal standard.

### Procedure for HDH of 4a

An 8 mL glass vial (Ø=14 mm, height 50 mm) equipped with a Teflon-coated oval magnetic stirring bar (8×5 mm) was charged with Ni-phen@TiO<sub>2</sub>-800 (25 mg) and ethyl 2-(4-bromophenyl)acetate **4a** (121.6 mg, 0.5 mmol) before the vessel was sealed with a plastic screw cap bearing a silicone septum. The silicone septum was then punctured with a 26-gauge syringe needle (0.45×12 mm). Triethylamine (88 µL, 0.625 mmol, 1.25 equiv) was then added via a 100 µL micro-syringe. A mixture of deionized water (0–1 mL) and ethanol (0–1 mL), or an alcoholic beverage (2 mL), was/were then added before the vial was placed into a small aluminum plate which was then transferred into a 300 mL steel autoclave (Parr Instrument Company). Once sealed, the autoclave was placed into a large aluminum heating block and purged 3 times with hydrogen (at 5–10 bar). Next the autoclave was pressurized with hydrogen (20 bar) and heated to 50 °C with thorough stirring (700 rpm). After 20 h, the autoclave was removed from the large aluminum block and cooled to room temperature in a water bath. The remaining hydrogen was discharged and the vials containing reaction products were removed from the autoclave. Ethyl acetate (6 mL) was added to the reaction vial and the resulting mixture was stirred intensively for 30 s. The solid catalyst was then separated by centrifugation and the liquid phase was analyzed by GC-FID to quantify the yield of **4b**, using *n*-hexadecane as an internal standard.

### Procedure for DDH

An 8 mL glass vial (Ø=14 mm, height 50 mm) equipped with a Teflon-coated oval magnetic stirring bar (8×5 mm) was charged with Ni-phen@TiO<sub>2</sub>-800 (25 mg) and 5-iodo-1,2,3-trimethoxybenzene **35a** (147.0 mg, 0.5 mmol) before the vessel was sealed with a plastic screw cap bearing a silicone septum. The silicone septum was then punctured with a 26-gauge syringe needle (0.45×12 mm). Triethylamine (88 µL, 0.625 mmol, 1.25 equiv) was then added via a 100 µL micro-syringe. Deionized water or D<sub>2</sub>O (1 mL) and methanol or methanol-*d*<sub>4</sub> (1 mL) were then added before the vial was placed into a small aluminum plate which was then transferred into a 300 mL steel autoclave (Parr Instrument Company). Once sealed, the autoclave was placed into a large aluminum heating block and purged 3 times with hydrogen or D<sub>2</sub> (at 3–5 bar). Next the autoclave was pressurized with hydrogen or D<sub>2</sub> (1 bar) and heated to 80 °C with thorough stirring (700 rpm). After 20 h, the autoclave was removed from the large aluminum block and cooled to room temperature in a water bath. The remaining hydrogen was discharged and the vials containing reaction products were removed from the autoclave. Ethyl acetate (6 mL) was added to the reaction vial and the resulting mixture was stirred intensively for



30 s. The solid catalyst was then separated by centrifugation and the supernatant was collected. The addition of ethyl acetate, vigorous stirring and collection was repeated a further two times. The combined ethyl acetate phases were filtered through diatomaceous earth (Celite) and then washed with a small amount of deionized water (2.5 mL) in a separatory funnel to remove  $\text{NEt}_3\text{-HI}$ . The organic phase was then dried over sodium sulfate before the solvent was removed by evaporation under reduced pressure. **35b** was dried overnight in vacuo, yielding an orange-brown solid. A sample was then dissolved in deuterated chloroform and analyzed by  $^1\text{H}$  NMR spectroscopy to determine the D-incorporation of **35b**.

## Acknowledgements

We gratefully acknowledge the support from the Federal Ministry of Education and Research (BMBF) and the State of Mecklenburg-Vorpommern. Financial support by Fonds der Chemischen Industrie (Kekulé-Stipendium no. 103231) for D. K. L. and Qatar National Research Fund (NPRP9-212-1-042) are also acknowledged. The authors thank Anja Simmula for ICP analyses and the analytical staff of the Leibniz Institute for Catalysis, Rostock, for their excellent service. QEERI Core Lab (Dr. S. Mansour, Dr. Y. Tong (XPS), Dr. A. R. Shetty (XRD), M. Helal (SEM) and J. Ponraj (TEM) are greatly acknowledged for analytical support and useful discussions. The authors thank Iryna Kazak for the accompanying illustration. Open Access funding enabled and organized by Projekt DEAL.

## Conflict of Interest

The authors declare no conflict of interest.

## Data Availability Statement

The data that support the findings of this study are available in the supplementary material of this article.

**Keywords:** heterogeneous catalysis · hydrodehalogenation · nickel · reduction · supported catalysts

- [1] a) B. Sahoo, A.-E. Surkus, M.-M. Pohl, J. Radnik, M. Schneider, S. Bachmann, M. Scalone, K. Junge, M. Beller, *Angew. Chem. Int. Ed.* **2017**, *56*, 11242–11247; *Angew. Chem.* **2017**, *129*, 11394–11399; B. Sahoo, A.-E. Surkus, M.-M. Pohl, J. Radnik, M. Schneider, S. Bachmann, M. Scalone, K. Junge, M. Beller, *Angew. Chem.* **2017**, *129*, 11394–11399; *Angew. Chem. Int. Ed.* **2017**, *56*, 11242–11247; b) A. Ramanathan, L. S. Jimenez, *Synthesis* **2010**, *2*, 217–220.
- [2] R. J. Thompson, *Ind. Eng. Chem.* **1932**, *24*, 620–623.
- [3] R. F. Addison, *Sci. Technol.* **1983**, *17*, 486 A–494 A.
- [4] a) H.-U. Blaser, *Adv. Synth. Catal.* **2002**, *1*, 344; b) K.-H. Kuck, U. Gisi, *Modern Crop Protection Compounds*, ed. W. Kramer, U. Schirmer, Wiley, Weinheim, **2007**, vol. 2, pp. 415–432; c) F. Earley, *Modern Crop Protection Compounds*, ed. W. Kramer, U. Schirmer, Wiley, Weinheim, **2007**, vol. 2, pp. 433–538.
- [5] R. Wilcken, M. O. Zimmermann, A. Lange, A. C. Joerger, F. M. Boeckler, *J. Med. Chem.* **2013**, *56*, 1363–1388.
- [6] O. Segev, A. Kushmaro, A. Brenner, *Int. J. Environ. Res. Public Health* **2009**, *6*, 478–491.
- [7] a) J. M. Stellman, S. D. Stellman, R. Christian, T. Weber, C. Tomasallo, *Nature* **2003**, *422*, 681–687; b) S. S. White, L. S. Birnbaum, *J. Environ. Sci. Health Part C* **2009**, *27*, 197–211; c) For an extensive review regarding the health effects of Agent Orange, see: *Veterans and Agent Orange: Update 2000*. The National Academies Press, Washington, DC, **2007**.
- [8] R. Ritter, M. Scheringer, M. MacLeod, C. Moeckel, K. C. Jones, K. Hungerbühler, *Environ. Health Perspect.* **2011**, *119*, 225–231.
- [9] B. R. Stanmore, *Combust. Flame* **2004**, *136*, 398–427.
- [10] H. I. Gomes, C. Dias-Ferreira, A. B. Ribeiro, *Sci. Total Environ.* **2013**, *445–446*, 237–260.
- [11] E. A. Paukshtis, L. G. Simonova, A. N. Zagoruiko, B. S. Balzhinimaev, *Chemosphere* **2010**, *79*, 199–204.
- [12] X. Chen, W. Ma, J. Li, Z. Wang, C. Chen, H. Ji, J. Zhao, *J. Phys. Chem. C* **2011**, *115*, 4089–4095.
- [13] Z.-L. Wu, B. Ondruschka, G. Cravotto, *Environ. Sci. Technol.* **2008**, *42*, 8083–8087.
- [14] C. Sun, S. A. Baig, Z. Lou, J. Zhu, Z. Wang, X. Li, J. Wu, Y. Zhang, X. Xu, *Appl. Catal. B* **2014**, *158–159*, 38–47.
- [15] a) C. Menini, C. Park, E.-J. Shin, G. Tavoularis, M. A. Keane, *Catal. Today* **2000**, *62*, 355–366; b) B. Léger, A. Nowicki, A. Roucoux, J.-P. Rolland, *J. Mol. Catal. A* **2007**, *266*, 221–225; c) F.-D. Kopinke, D. Angeles-Wedler, D. Fritsch, K. Mackenzie, *Appl. Catal. B* **2010**, *96*, 323–328; d) R. Navon, S. Eldad, K. Mackenzie, F.-D. Kopinke, *Appl. Catal. B* **2012**, *119–120*, 241–247.
- [16] F. Alonso, I. P. Beletskaya, M. Yus, *Chem. Rev.* **2002**, *102*, 4009–4091.
- [17] a) R. Ueno, T. Shimizu, E. Shirakawa, *Synlett* **2016**, *27*, 741–744; b) Y. Ukisu, T. Miyadera, *J. Mol. Catal. A* **1997**, *125*, 135–142; c) H.-X. Zheng, X.-H. Shan, J.-P. Qu, Y.-B. Kang, *Org. Lett.* **2017**, *19*, 5114–5117.
- [18] R. C. Larock, S. Ding, *Tetrahedron Lett.* **1993**, *34*, 979–982.
- [19] a) B. H. Lipshutz, T. Tomioka, K. Sato, *Synlett* **2001**, *SI*, 970–973; b) C. Rettenmeier, H. Wadepohl, L. H. Gade, *Chem. Eur. J.* **2014**, *20*, 9657–9665; c) H. Parnes, J. Pease, *J. Org. Chem.* **1979**, *44*, 151–152.
- [20] a) H. Guo, K.-I. Kanno, T. Takahashi, *Chem. Lett.* **2004**, *33*, 1356–1357; b) H. Ryuichiro, S. Wen-Hua, N. Yasushi, T. Tamotsu, *Chem. Lett.* **1997**, *26*, 1251–1252; c) R. Hara, K. Sato, W.-H. Sun, T. Takahashi, *Chem. Commun.* **1999**, *12*, 845–846.
- [21] B. Singh, J. Ahmed, A. Biswas, R. Paira, S. K. Mandal, *J. Org. Chem.* **2021**, *86*, 7242–7255.
- [22] X. Ma, S. Liu, Y. Liu, G. Gu, C. Xia, *Sci. Rep.* **2016**, *6*, 25068.
- [23] P. T. Anastas, J. C. Warner, *Green Chemistry: Theory and Practice*, Oxford University Press, Oxford, **1998**, pp. 30.
- [24] a) P. Ryabchuk, G. Agostini, M.-M. Pohl, H. Lund, A. Agapova, H. Junge, K. Junge, M. Beller, *Sci. Adv.* **2018**, *4*, eaat0761; b) F. Chen, C. Kreyenschulte, J. Radnik, H. Lund, A.-E. Surkus, K. Junge, M. Beller, *ACS Catal.* **2017**, *7*, 1526–1532; c) F. Chen, B. Sahoo, C. Kreyenschulte, H. Lund, M. Zeng, L. He, K. Junge, M. Beller, *Chem. Sci.* **2017**, *8*, 6239–6246; d) B. Sahoo, D. Formenti, C. Topf, S. Bachmann, M. Scalone, K. Junge, M. Beller, *ChemSusChem* **2017**, *10*, 3035–3039; e) D. Formenti, F. Ferretti, C. Topf, A.-E. Surkus, M.-M. Pohl, J. Radnik, M. Schneider, K. Junge, M. Beller, *J. Catal.* **2017**, *351*, 79–89; f) P. Ryabchuk, A. Agapova, C. Kreyenschulte, H. Lund, H. Junge, K. Junge, M. Beller, *Chem. Commun.* **2019**, *55*, 4969–4972.
- [25] N. D. Jablonowski, A. Schäffer, P. Burauel, *Environ. Sci. Pollut. Res. Int.* **2011**, *18*, 328–331.
- [26] a) K. Sanderson, *Nature* **2009**, *458*, 269; b) A. Katsnelson, *Nat. Med.* **2013**, *19*, 656; c) C. Schmidt, *Nat. Biotechnol.* **2017**, *35*, 493–494.
- [27] a) W. Li, R. Liang, A. Hu, Z. Huang, Y. N. Zhou, *RSC Adv.* **2014**, *4*, 36959–36966; b) A. Hu, X. Zhang, D. Luong, K. D. Oakes, M. R. Servos, R. Liang, S. Kurdi, P. Peng, Y. Zhou, *Waste Biomass Valorization* **2012**, *3*, 443–449; c) A. Meng, J. Zhang, D. Xu, B. Cheng, J. Yu, *Appl. Catal. B* **2016**, *198*, 286–294.
- [28] W. Liu, Y. Zhang, *J. Mater. Chem. A* **2014**, *2*, 10244–10249.
- [29] a) J. Jitputti, S. Pavasupree, Y. Suzuki, S. Yoshikawa, *Jpn. J. Appl. Phys.* **2008**, *47*, 751–756; b) X. Zhao, W. Jin, J. Cai, J. Ye, Z. Li, Y. Ma, J. Xie, L. Qi, *Adv. Funct. Mater.* **2011**, *21*, 3554–3563.
- [30] a) J. Li, P. Li, J. Li, Z. Tian, F. Yu, *Catalysts* **2019**, *9*, 506; b) L. A. García-Cerda, K. M. Bernal-Ramos, S. M. Montemayor, M. A. Quevedo-López, R. Betancourt-Galindo, D. Bueno-Báques, *J. Nanomater.* **2011**, *2011*, 162495.
- [31] W. Zhang, B. Li, *Int. J. Electrochem. Sci.* **2018**, *13*, 3516–3526.
- [32] a) M. C. Biesinger, B. P. Payne, L. W. M. Lau, A. Gerson, R. S. C. Smart, *Surf. Interface Anal.* **2009**, *41*, 324–332; b) A. M. Hengne, A. K. Samal, L. R. Enakonda, M. Harb, L. E. Gevers, D. H. Anjum, M. N. Hedhili, Y. Saih, K.-W. Huang, J.-M. Basset, *ACS Omega* **2018**, *3*, 3688–3701.



- [33] a) S. Sakthivel, H. Kisch, *Angew. Chem. Int. Ed.* **2003**, *42*, 4908–4911; b) H. Wang, Z. Wu, Y. Liu, *J. Phys. Chem. C* **2009**, *113*, 13317–13324; c) L. Zhang, R. V. Koka, *Mater. Chem. Phys.* **1998**, *57*, 23–32; d) J. Liu, Q. Zhang, J. Yang, H. Ma, M. O. Tade, S. Wang, J. Liu, *Chem. Commun.* **2014**, *50*, 13971–13974.
- [34] a) R. Purbia, R. Borah, S. Paria, *Inorg. Chem.* **2017**, *56*, 10107–10116; b) Y. Koshtyal, D. Nazarov, I. Ezhov, I. Mitrofanov, A. Kim, A. Rymyantsev, O. Lyutakov, A. Popovich, M. Maximov, *Coating* **2019**, *9*, 301.
- [35] a) F. Jaouen, J. Herranz, M. Lefèvre, J.-P. Dodelet, U. I. Kramm, I. Herrmann, P. Bogdanoff, J. Maruyama, T. Nagaoka, A. Garsuch, J. R. Dahn, T. Olson, S. Pylypenko, P. Atanassov, E. A. Ustinov, *ACS Appl. Mater. Interfaces* **2009**, *1*, 1623–1639; b) B. J. Matsoso, K. Ranganathan, B. K. Mutuma, T. Leretholi, G. Jones, N. J. Coville, *RSC Adv.* **2016**, *6*, 106914–106920.
- [36] Y. Wang, L. Li, X. Huang, Q. Li, G. Li, *RSC Adv.* **2015**, *5*, 34302–34313.

---

Manuscript received: October 28, 2021  
Revised manuscript received: December 16, 2021  
Accepted manuscript online: January 3, 2022  
Version of record online: January 27, 2022